Quantifying the influence of conduit inclination on Taylor Bubble behaviour in basaltic magmas.

Hannah Calleja[1] & Tom D. Pering[1*]

[1]Department of Geography, University of Sheffield
[*]Corresponding author: t.pering@sheffield.ac.uk, @tompering

This is a non-peer reviewed preprint submitted to EarthArXiv.

Quantifying the influence of conduit inclination on Taylor Bubble behaviour in basaltic magmas.

Calleja, H[1]., Pering, T.D[1*].

[1]Department of Geography, Sheffield, University of Sheffield, S10 2TN, United Kingdom

[*]Corresponding Author, t.pering@sheffield.ac.uk

Abstract:

The ascent of single Taylor bubbles suspended in a range of Newtonian liquids, scaled to mimic basaltic magmas, within vertical and inclined tubes has been studied experimentally over the range 0° to 70° (where 0° is vertical and 90° is horizontal). Using measurements of Taylor bubble parameters (ascent velocity and film thickness) and morphology, alongside dimensionless numbers, we show that inclination has a clear effect on bubble behaviour and morphology. Notably, ascent velocity peaks at inclinations of 40 to 50°, with proportional velocity increases of ~40-90% with respect to vertical ascent values, before decreasing again. This work provides a basis for the expansion of existing theoretical framework to accommodate for conduit inclination in volcanic scenarios.

1. Introduction

Developing the theoretical frameworks of gas-magma dynamics in volcanic conduits is a fundamental aspect to the understanding of basaltic activity dynamics worldwide (Seyfried and Freundt, 2000). Such activity can range from quiescent passive activity through to the end member of lava fountaining from vents or fissures (Parfitt, 2004; Parfitt and Wilson, 1995). Key to understanding the drivers of these styles of activity are the gas flow regimes in the conduit, and how individual bubbles may interact and travel during ascent (Sparks, 2003, 1978), none more so than one of the most common classes of basaltic activity, the strombolian eruption (Blackburn et al., 1976; Parfitt, 2004; Taddeucci et al., 2015). This class of basaltic activity involves the discrete ejection of incandescent pyroclasts, often alongside an ashy component, driven by the rapid expansion of Taylor bubbles (also known as gas slugs) as they reach the surface.

The morphology and behaviour of Taylor bubbles in relation to basaltic style activity has been a major focus, e.g., (James et al., 2009; Kawaguchi and Nishimura, 2015; Pering et al., 2016; Pering and McGonigle, 2018; Seyfried and Freundt, 2000; Spina et al., 2013), however, the formation of Taylor bubbles is also key, with different mechanisms allowing for differences in ascent times and hence affecting activity development. The classic formation mechanisms invoked are the rise speed

dependent model (Parfitt, 2004; Parfitt and Wilson, 1995; Wilson and Head, 1981) and the collapsing foam model (Jaupart and Vergniolle, 1988; Vergniolle and Jaupart, 1990, 1986). However, more recent work explores system complexities through the influence of crystal packing (Woitischek et al., 2020), rheological changes in the magma via viscous caps (Barth et al., 2019; Capponi et al., 2016; Del Bello et al., 2015) or a combination of the two (Oppenheimer et al., 2020), and finally through cascade coalescence of trains of ascending Taylor bubbles (Pering et al., 2017; Pering and McGonigle, 2018).

The structure and characteristic behaviours, e.g., ascent velocities, film thickness, and stability of Taylor bubbles ascending in vertical conduits has been described in detail by several previous works (Bugg and Saad, 2002; Campos and Carvalho, 1988; de Azevedo et al., 2016; Llewellin et al., 2012; Viana et al., 2003). The bubble is split into four major components (Figure 1): (1) the nose is the uppermost part of the bubble and its approximately hemispherical structure remains widely unchanged between bubble and liquid types, (2) the main body which is surrounded by a falling liquid film and remains relatively stable throughout bubble ascent (Llewellin et al., 2012), (3) the tail, and (4) the wake. The body is further subdivided into (2a) the upper portion, where the film thickness accelerates and thins as it develops, and (2b) the lower portion, where the film has a steady thickness because the forces acting on it are in equilibrium. Tail morphology varies depending on regime stability and the wake can be classified as open, closed, or turbulent (Campos and Carvalho, 1988; Nogueira et al., 2006; Pinto et al., 1998).

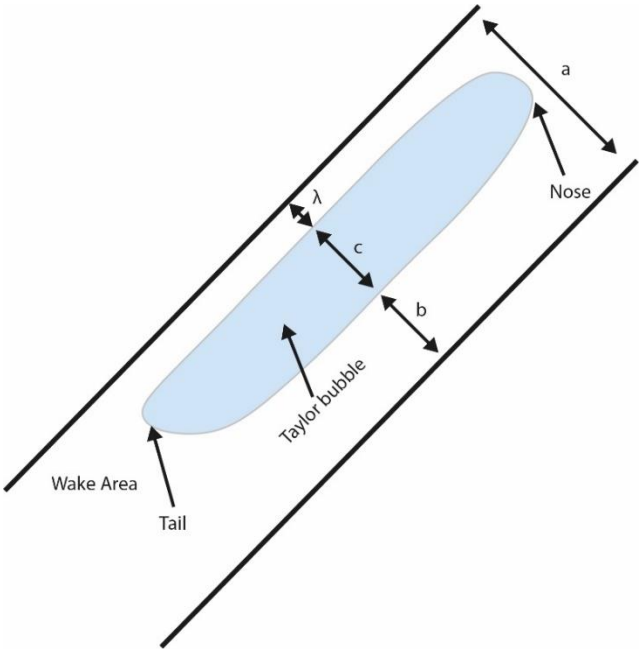

Figure 1: A diagram showing the key features of a Taylor bubble in an inclined tube. Also highlight is the measurement technique for falling film thickness, λ; a = internal tube diameter; b = the lower film thickness; c = bubble width. $\lambda = a - (b+c)$.

Quantitative experimental data for Taylor bubble ascent velocity and thickness of the falling film rising around Taylor bubbles in inclined tubes are far scarcer. James et al., (2004) investigated the dependence of flow patterns on tube inclination within a volcanic context, showing the effect of in-conduit pressure fluctuations on the formation of large individual slugs, highlighting, the promotion of Taylor bubble flow from bubbly as inclination moves from 0 to ~ 30°.

Engineering applications such as bubble column reactors and transport pipelines have driven a comprehensive literature for two-phase flow in inclined tubes filled for Newtonian fluids (Shosho and Ryan, 2001). Zukoski (1966) can be attributed as one of the first studies to investigate the effects of tube inclination on Taylor bubble rise velocity using an experimental approach.

In this study, using a low-cost experimental approach, we address this gap in the theoretical literature covering the ascent of Taylor bubbles in inclined conduits, scaled to basaltic magmas. This study is of importance given that non vertical conduits are likely commonplace at strombolian explosion exhibiting locations, e.g., (Chouet et al., 1997; Ilanko et al., 2015; James et al., 2004).

Table 1: Summary of existing experimental studies for slug ascent in vertical and inclined tubes.

Author	Field of study	Inclination	Experimental approach	Summary
Zukoski (1966)	Engineering	Inclined, range unknown.	Tube-draining air and liquid bubbles in water, carbon tetrachloride, mercury, glycerine and ethylene glycol solutions.	Discussed influence of viscosity and surface tension on bubble rise, and the influence of tube inclination.
Bendiksen (1984)	Engineering	-30° to 90°*	Finite slugs in water.	Proposed a correlation to estimate influence of inclination on slug ascent.
Campos and de Carvalho (1988)	Volcanology	Vertical	Dyed red liquid; gas-air two phase flow.	Photographic study of wake behaviour in different tube diameters.
Nigam et al., (1995)	Engineering	30° to 90°*	CO_2 bubbles in closed tubes.	Effect of inclination on single slug rise velocity and liquid-phase controlled mass transfer.
Bugg et al., (1997)	Engineering	Vertical	Large cylindrical & spherical bubbles into infinite-quiescent fluid.	Numerical investigation using a 2D transient finite difference model to track slug movement.
Seyfried and Freundt (2000)	Volcanology	Vertical	Tubes had in-built obstacles to encourage gas pocket formation.	Simulate multi-phase flow and subsequent eruptive behaviour focussing on slug and annular flow.

Shosho and Ryan (2001)	Engineering	5, 15, 30, 45, 60, 75 and 90°	Tube-draining bubbles in Newtonian and non-Newtonian fluids.	Gives Fr as a function of inclination angle and Eo.
Viana et al., (2003)	Engineering	Vertical	Long gas bubbles in stagnant fluids.	Provides a universal correlation for slug ascent velocity from published and own data.
James et al., (2006)	Volcanology	Vertical & inclined.	Different tube diameters used for slug ascent.	Systematic pressure changes varying with slug size, liquid depth, tube diameter and fluid viscosity were observed.
Pokusaev et al., (2011)	Engineering	0° to 90° *	Tube diameters 11.8, 18 and 30 mm. Air bubbles in water and an immersion liquid.	Describes bubble velocity as a function of changing nose morphology with inclination.
Llewellin et al., (2012)	Engineering	Vertical	Slugs in water, soap and oil solutions.	Provides theoretical basis for applying dimensionless quantities to slug parameters.
De Azevedo et al., (2015)	Engineering	0, 2.5, 5, 7.5, 10, and 15°	Air bubbles rising in water-glycerine mixtures.	Measures the shape of Taylor bubbles using a pulse-echo ultrasonic technique.

2. Methods

This study examines the Taylor bubble ascent process in vertical and inclined tubes using an existing and repeatable experimental approach based on previous studies from volcanic, fluid dynamics and chemical engineering backgrounds (summarised in Table 1). To achieve this, clear, cylindrical, and open-ended acrylic tubes of 1 m in length and two internal diameters (0.016 m and 0.027 m) were suspended using two clamp stands to stabilise the equipment (Figure 2). A clinometer was used to measure the angle to which the tubes were inclined, ranging from 0° (vertical) to 40° in 10° increments, then from 45° to 70° in 5° increments, tailored to where an observable change in Taylor bubble behaviour occurred during testing. This range of values covers the inclinations that are representative of existing volcanic conduits as seen in a range of literature. For example, Chouet et al., (1997) detail an approximate conduit inclination of 40° from vertical at Stromboli, while Chouet et al., (2003) and James et al., (2004) also conducted a similar investigation at inclinations of roughly 30°.

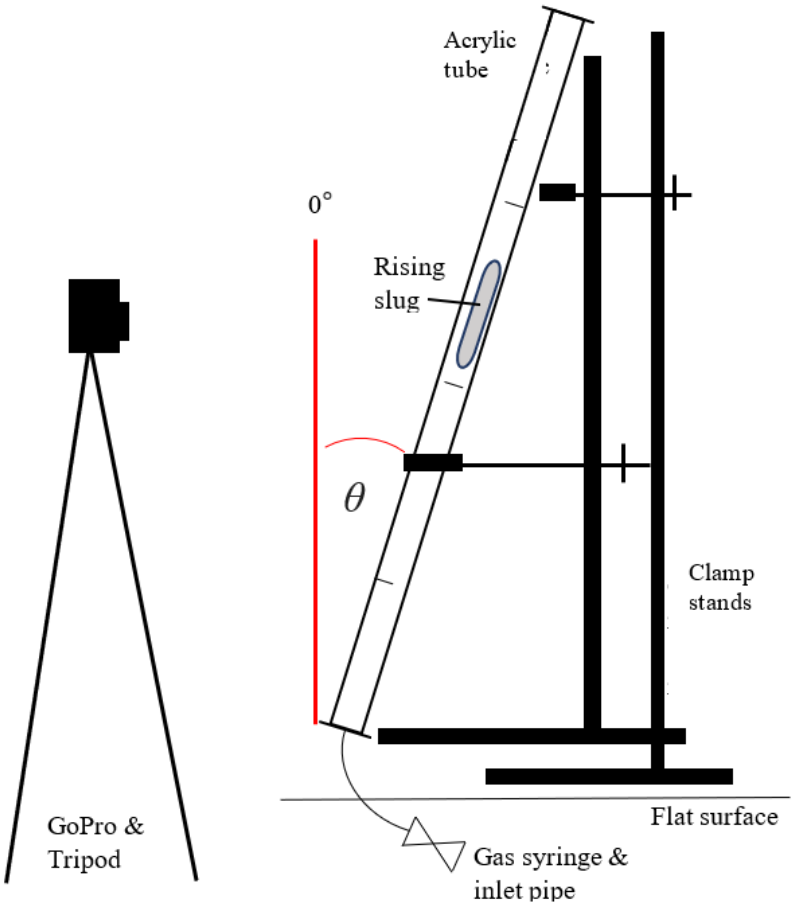

Figure 2: Experimental set-up for all data collection (left); a marked distance of 25cm is shown by perpendicular lines on the tube and θ denotes the angle measured from vertical (see also individual labels).

Each tube was then filled with Newtonian liquids (see Table 2) to approximately 90% capacity to prevent spillage once the Taylor bubble was introduced, especially as tubes were inclined closer to the horizontal. Single Taylor bubbles were injected into the tubes using a gas syringe which was attached to the base of the pipe via rubber tubing. Injected gas volumes were kept constant for each tube diameter, using a 10 ml and 50 ml gas syringe for the 0.016 m and 0.027 m diameter tubes, respectively, ensuring that slug length was >1.5D (D = tube diameter) where bubble velocity is independent of slug length (Shosho and Ryan, 2001). Taylor bubble ascent was recorded using a tripod-mounted GoPro which was positioned parallel to the centre point of each tube to minimise camera distortion. Separate recordings for each bubble ascent were made a total of ten times per inclination for each liquid other than with golden syrup, where five repeats per inclination were recorded as its high viscosity severely inhibited ascent times. To prevent fluid mixing in between runs, tubes were rinsed thoroughly with soap and water then dried using compressed air.

Table 2: Summary of Newtonian liquid properties and N_f number.

	Water	*Sunflower oil*	*Olive oil*	*Glycerol*	*Golden Syrup*
Density (kg m^3)	997	898	902	1266	1438
Viscosity (Pa s)	0.00089	0.123	0.129	0.416	18.35
Surface tension (mN m^{-1})*	72.86	34	33	64	80
N_f at D = 0.016 m	7101	46	44	19	0.5
N_f at D = 0.027 m	15566	101	97	42	1.1

** existing values*

The tubes were filled with a set of Newtonian liquids: water, sunflower oil, olive oil, glycerol and golden syrup, all of which are low cost, non-toxic and readily available fluids. The density and viscosity of each liquid (Table 2) were then calculated. Liquid density, ρ was determined by calculating the weight of 100 ml of each liquid then substituting the values into the equation:

$$\rho = \frac{m}{V} \qquad (1)$$

where m is the mass of the liquid and V is the volume of the liquid. The viscosity (μ) of each liquid was calculated by dropping a steel ball into a 1 litre measuring cylinder, then calculating the fall velocity over 20 cm, and applying the following:

$$\mu = \frac{2(\rho_s - \rho)ga^2}{9v} \qquad (2)$$

where ρ_s is the density of the sphere, ρ is the liquid density, g is acceleration due to gravity, a is the radius of the sphere and v is the velocity of the sphere. Each displayed value for liquid density and viscosity (Table 2 is the average of three measurements.

Taylor bubble velocities were measured individually for each repeat of each inclination for all liquids, using ImageJ (https://imagej.nih.gov/ij/). Ascent velocity (v_b) was calculated by measuring the time taken for the tip of the nose to cover a marked distance of 50 cm (Figure 2):

$$v_b = \frac{d}{t} \qquad (3)$$

where v_b is bubble velocity, d is distance travelled and t is time. Taylor bubble ascent was measured over the central part of the tube (from the 25 to 75 cm marks) as ascent velocity reaches a steady value within five to ten radii of gas injection then remains constant, assuming there is no outside interference (Llewellin et al., 2012). In the case that the bubble had not fully formed or stabilised before reaching

25 cm the ascent time was instead measured between 50 and 75 cm, i.e., for glycerol and golden syrup, as bubble length increased in liquids of a higher viscosity, while inclination had a further lengthening effect on slug morphology.

To measure the thickness of the falling film, λ, in inclined tubes, the bubble width was added to the width of the lower film thickness (i.e., in an inclined tube the bubble ascends closer to the upper tube wall) then the total was subtracted from the internal diameter (Figure 1). Falling film thickness was measured in vertical tubes by subtracting bubble width from internal tube diameter then halving the resulting value because falling films present symmetry in all directions around the bubble when the condition of the surrounding tube is vertical (de Azevedo et al., 2015).

3. Results and Discussion

3.1. Theoretical Framework

Calculating the flow parameters of the Taylor bubbles allows for the development of our understanding of flow structure and movement while specifically providing a way to describe observed behaviour numerically at both laboratory and volcanic scales. The ascent velocity of Taylor bubbles, v_b, in vertical tubes has been shown to be dependent on the liquid density ρ, viscosity μ, gravitational acceleration g, the liquid-gas interfacial tension σ, and the internal diameter of the tube D (Llewellin et al., 2012). These values have been combined to form dimensionless quantities, which are used to describe the behaviour of fluids. These include the Froude number:

$$Fr = \frac{v_b}{\sqrt{gD}}, \qquad (4)$$

the Eotvos number:

$$Eo = \frac{\rho g D^2}{\sigma}, \qquad (5)$$

and the Reynolds number:

$$Re = \frac{\rho v_b D}{\mu} \qquad (6)$$

The Froude number is a dimensionless velocity describing flow pattern over an obstacle, or the ratio of inertial and gravitational (buoyancy) forces. The Eotvos number, describes the importance of gravitational (buoyancy) forces, compared to surface tension forces. The Reynolds number represents the ratio of inertial and viscous forces in the liquid to help predict flow patterns in various

fluid flow situations, especially in relation to turbulence and its implications on bubble formation and stability. A fourth parameter has also been calculated using the liquid property values; this is the dimensionless inverse viscosity (N_f):

$$N_f = \frac{\rho\sqrt{gD^3}}{\mu} \qquad (7)$$

which represents the ratio of external to internal forces and liquid flow pattern in the wake.

Taylor bubble parameters, from our experiments, have been described as seen in Figures 3 to 13, where v_b, *Fr*, *Eo*, *Re*, and λ are plotted as functions of tube inclination angle θ. Each solid line corresponds to a particular tube diameter *D*, and each subplot shows data for a different Newtonian fluid. For the sake of comparison to a volcanic scale, the range of dimensionless values covered by this study are: $1.2 \times 10^{-3} \leq Re \leq 7.9 \times 10^{3}$, $3.1 \times 10^{-3} \leq Fr \leq 5.4 \times 10^{-1}$, and $0.5 \leq N_f \leq 1.5 \times 10^{4}$. The ranges calculated in cover the known range of estimated dimensionless parameters at real volcanic conduits (Tables 2 and 3), with water and golden syrup acting as appropriate endmembers while the remaining liquids ($19.3 \leq N_f \leq 101$) likely encompass the magmatic range for inverse viscosity observed at volcanoes such as Stromboli and Yasur (Table 3).

Table 3: Summary of relevant parameters for existing volcanoes. Conduit diameter is listed beneath each volcano. It is assumed that surface tension = 0.4 and conduit geometry is vertical.

Volcano	N_f	*Re*	*Fr*	*Eo*	$v_b\ (ms^{-1})$
Erebus *3 - 6 m*	4.067 – 11.502	1.427 – 4.037	0.4 – 0.11	551812 - 981000	0.22 – 0.84
Yasur *1.5 - 3 m*	14.953 – 42.293	5.248 – 14.845	0.13 – 0.24	143171 - 573885	0.5 – 1.3
Stromboli *1.5 m*	51.760	18.168	0.26	148989	1.0
Masaya *1.5 - 6 m*	517.598 – 4140.783	181.677 – 1453.415	0.34*	148989 - 2383830	1.3 – 2.6

*reached ~0.35 constant as proposed in Llewellin et al., (2012).

As a function of inclination (excluding falling film thickness), all dimensionless attributes follow the same trend: as inclination angle increases from a vertical ($\theta = 0°$) position they increase to a maximum

value, typically within the range of 40° to 60°, then decrease. All relationships are shown to be non-linear, with trends relating to inclination that agree with results from previous chemical engineering literature (Bendiksen, 1984; Shosho and Ryan, 2001; Nigam et al., 1995; Pokusaev et al., 2011; Zukoski, 1966).

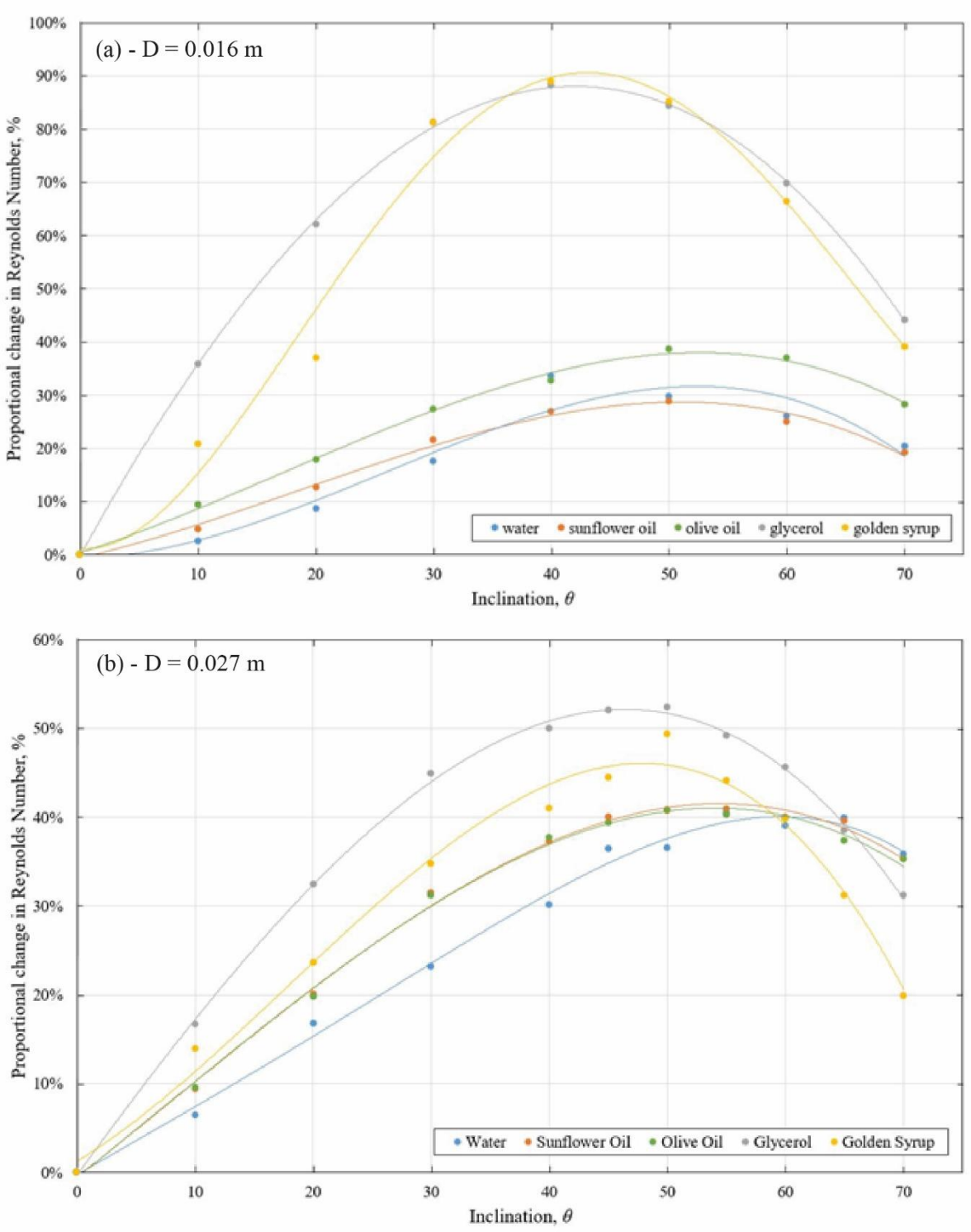

Figure 3: Proportional change in Reynolds number as a function of tube inclination for (a) D = 0.016 and (b) D = 0.027 m for all liquids.

3.2. Reynolds Number

High Reynolds numbers coincide with high N_f values, and higher Reynolds numbers are indicative of turbulence, therefore smaller values for *Re* occur at low N_f, where the flow regime is observed to be laminar. According to Campos and Carvalho (1988) wake shape is axisymmetric when $Re < 180$; this also applies to the results for this study within the range $0.5 \leq N_f \leq 101$, i.e., all liquids but water. Existing studies (Amaya-Bower and Lee, 2010; Campos and Carvalho, 1988) observe oscillation in the wake to occur within the range $180 \leq Re \leq 304$, which somewhat agrees with observations in this study, although it is difficult to determine the exact threshold for the onset of turbulent flow as the values within this range are not explicitly covered by this dataset.

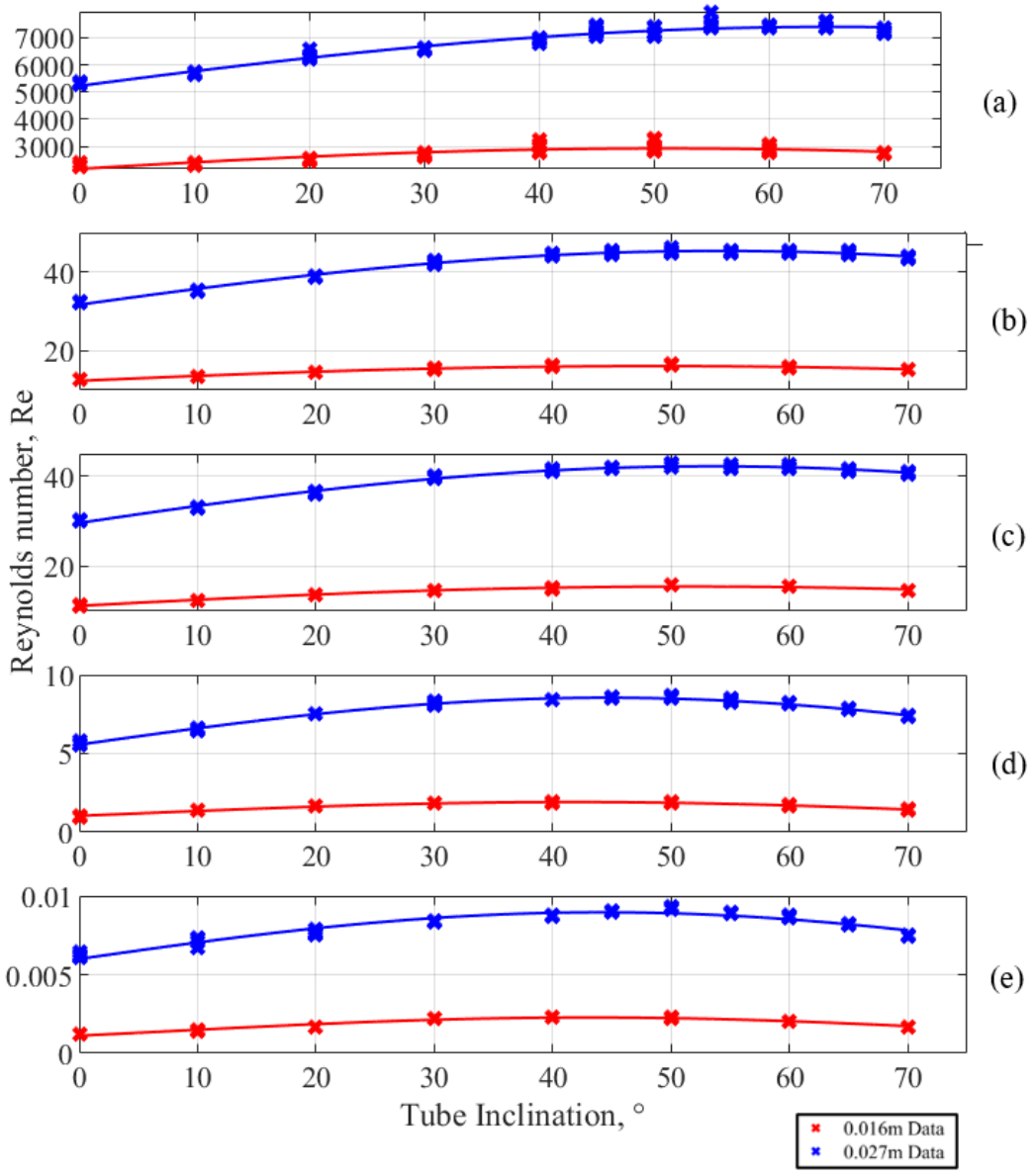

Figure 4: Reynolds number as a function of tube inclination for both tube diameters in various Newtonian liquids: water (a), sunflower oil (b), olive oil (c), glycerol (d), and golden syrup (e).

For D = 0.016 m and $N_f \leq 20$ (approximately), *Re* exhibits a proportional increase of 80 – 90% at the maxima, which occurs where θ = ~40 (Figure 3a). This is not as pronounced at D = 0.027 m, where the highest proportional change in *Re* occurs in glycerol (N_f = 42.3, D = 0.027 m) within the range $45 < \theta < 50$ (Figure 3b). The dependence of the Reynolds number on inclination angle decreases as viscous effects increase for all inclinations but vertical, especially in liquids of the lowest N_f at D = 0.016 m. More viscous liquids show a wider range of values overall and the greatest maximum occurs in the wider tube diameter (Figure 3b). The maximum proportional change shifts from ~40° (glycerol and golden syrup) to ~55° (sunflower and olive oil) to ~60° (water) for D = 0.016 m (Figure 3a). Sunflower and olive oil have very similar rates of proportional change in *Re* for both diameters (although more so for D = 0.027 m), likely due to having similar liquid properties. As indicated by the results (Figure 4), the Reynolds number is very sensitive to variations in viscosity; this is also reflected in equation (6), meaning that in vertical tubes *Re* is a function of N_f only (in agreement with literature), however, it also becomes a function of tube inclination for $\theta > 0$.

3.3. Froude Number

Fr increases when θ increases from vertical until a maximum is reached within the range $45 \leq \theta \leq 65$, then decreases for all fluids (Figure 5). These results agree with the qualitative behaviour for Froude number as a function of inclination observed (Shosho and Ryan, 2001; Zukoski, 1966). Tube diameter has a significant and complex effect on Froude number; as liquid viscosity increases (and N_f decreases) *Fr* values decrease; this occurs to a more significant extent for D = 0.016 m than for D = 0.027m with glycerol and golden syrup. Specifically, for D = 0.016 m containing water, *Fr* is higher than for D = 0.027 m; for the range $44 \leq N_f \leq 101$ (encompasses both oils). *Fr* values from both diameters are similar; then for the range $0.5 \leq N_f \leq 42$ (glycerol and golden syrup) *Fr* is higher in D = 0.027 m than in D = 0.016 m. Shosho and Ryan (2001) propose that this occurs for $N_f \leq 50$ (approximately), which agrees with the results seen here (glycerol and golden syrup). For both tube sizes the fluid with $0.5 \leq N_f \leq 1.1$ (golden syrup) exhibited *Fr* values well below those seen in other liquids. The literature (Shosho and Ryan, 2001; Bugg and Saad, 1998; Llewellin et al., 2012) state that *Fr* has a constant value of $Fr \approx 0.351$ in vertical tubes when viscous forces and surface tension forces are negligible ($N_f > 300$ and $Eo > 100$). This constant is also applied to real volcanic conduits: Table 3 demonstrates that this occurs at Masaya Volcano in Nicaragua, where Fr = 0.34 remains constant for D = 1.5 – 6 m, where at volcanoes with more viscous magmas ($N_f < 300$) such as Erebus and Yasur, *Fr*

increases with increasing conduit diameter. The results of this study also reflect this constant in liquids of high N_f (water, sunflower oil and olive oil), where the range $0.3 \leq Fr \leq 0.4$ is observed in vertical tubes, consistent with potential flow theory (Bugg and Saad, 2002) and values in other literature (Seyfried and Freundt, 2000; Shosho and Ryan, 2001; Viana et al., 2003; Llewellin et al., 2012). However, overall values for Fr calculated in this study were in the range $3.1 \times 10^{-3} < Fr < 5.4 \times 10^{-1}$ for the full range of N_f, where the highest Froude number occurred within inclined tubes for $45 \leq \theta \leq 55$ (Figure 5) and the lowest Froude numbers occurred in vertical tubes where $D = 0.016$ m for the lowest N_f. Even in the case of $N_f > 300$, Fr values exceeded the constant of $Fr \approx 0.351$ when inclination angle was greater than 0°. Pokusaev et al., (2011) alludes to an explanation for this complex behaviour when it is stated that the constant is upheld within a system that is in inertial control, i.e., when liquid flow is laminar and the shape of the bubble nose is hemispherical, which is not the case in inclined tubes.

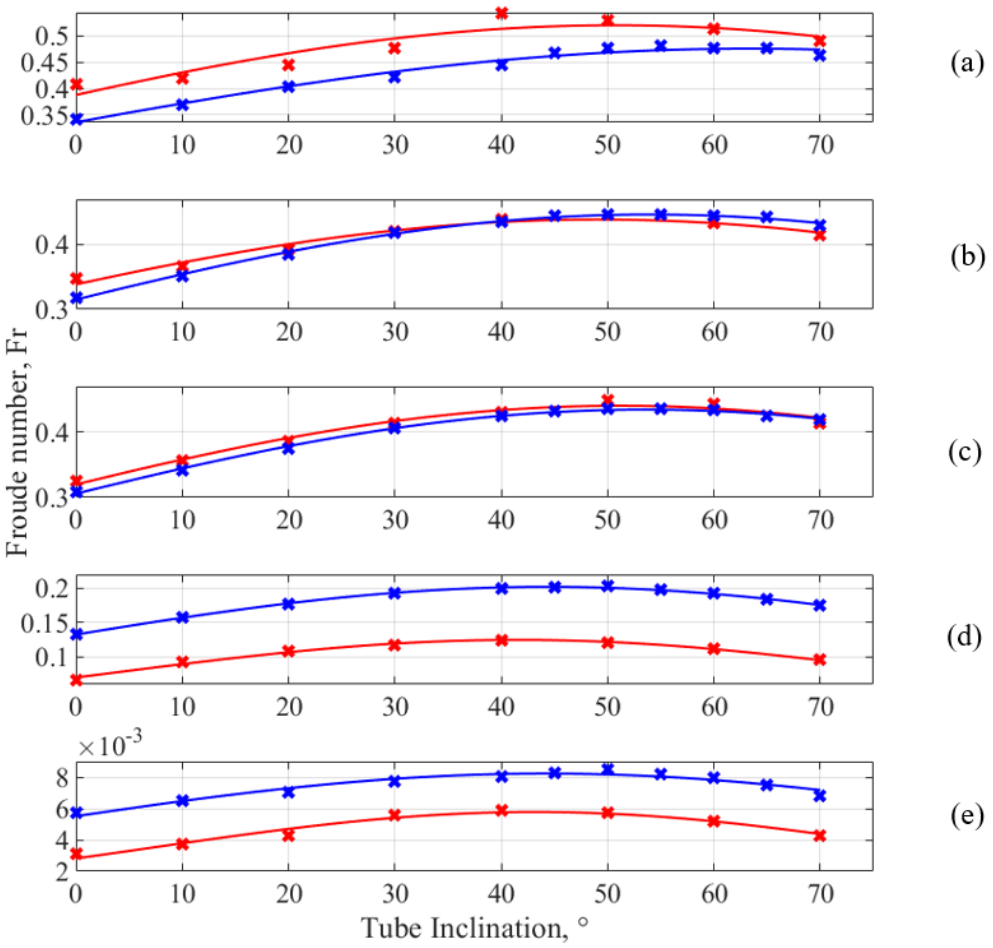

Figure 5: Froude number as a function of tube inclination for both tube diameters in various Newtonian liquids: water (a), sunflower oil (b), olive oil (c), glycerol (d), and golden syrup (e).

3.4. Film Thickness and Interfacial Tension

The data collected for film thickness in this study refers to the 'upper falling film thickness', i.e., that located on the upper side of the Taylor bubble where it comes into close contact with the upper wall of the tube. This deviation away from the central axis of the tube occurs because of the buoyancy or level effects acting on the bubble. As a result of this, the 'lower film thickness', which refers to the film thickness on the opposite side of the bubble, increases to a maximum with increasing tube angle and decreasing N_f. As with Llewellin et al., (2012), in this study it is not assumed that the falling film is uniformly thin, so λ is used to denote film thickness instead of the conventional use of δ.

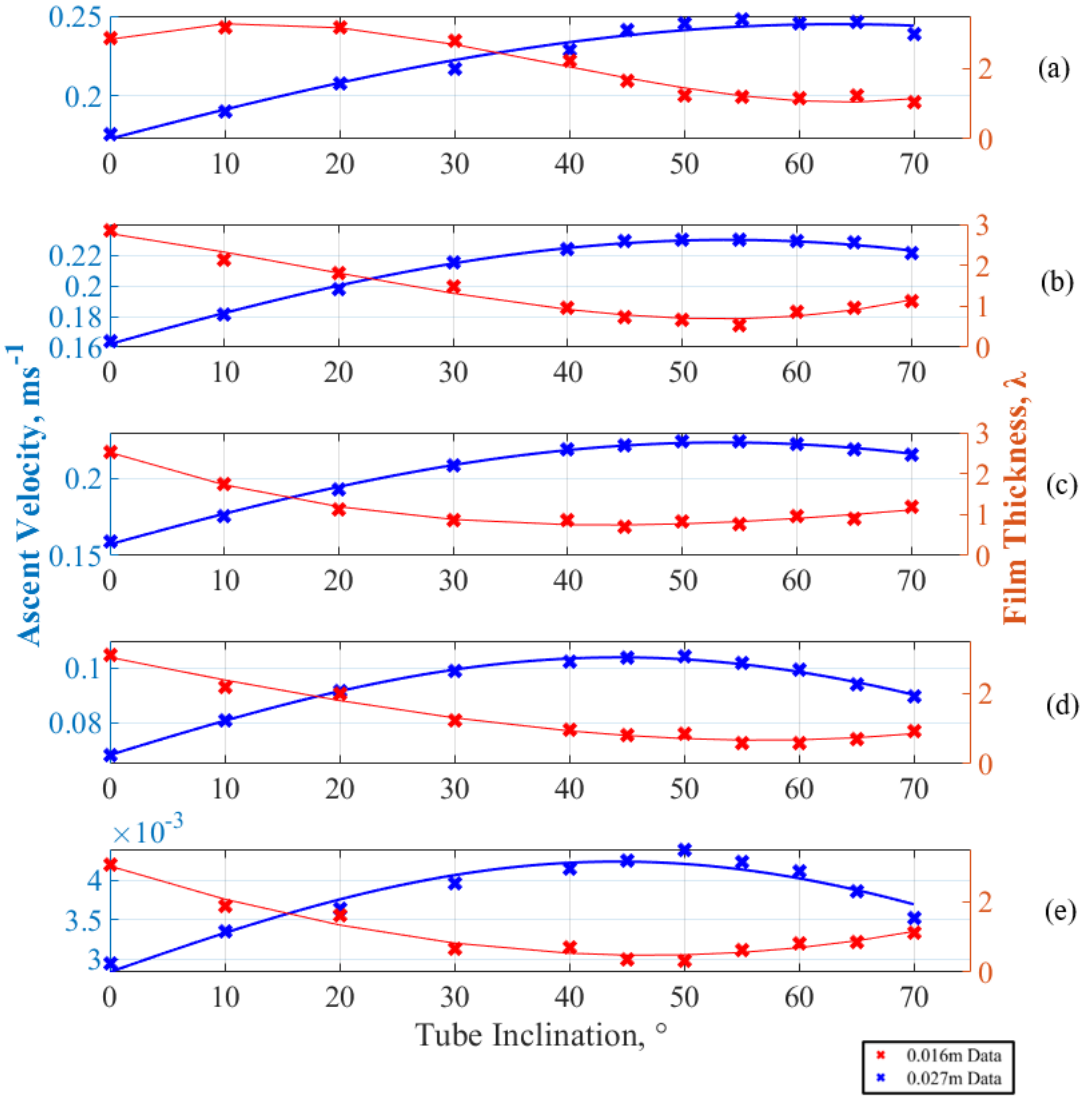

Figure 6: Slug ascent velocity (blue) and falling film thickness (red) as a function of tube inclination for D = 0.027 m in various Newtonian liquids: water (a), sunflower oil (b), olive oil (c), glycerol (d), and golden syrup (e).

Falling film thickness has an inverse relationship with all other measured parameters (Figure 6). Except for water, film thickness decreases with increasing inclination until a minimum value is reached within the range of $45 \leq \theta \leq 55$ (in line with the maxima of all other parameters) before increasing again as inclination approaches 70° for the range $0.5 \leq Nf \leq 101$. Llewellin et al., (2012) states that surface tension may play a different role in controlling film thickness (and therefore rise velocity) for transitional and turbulent films. This can be observed in Figure 7 where the relationship of *Eo* and film thickness as a function of inclination appears sigmoidal in nature for high N_f values (water) as inclination increases from the vertical. The significance of this was not investigated further due to a lack of available data for high N_f but may be a result of a breakdown of the thin film assumption (Pokusaev et al., 2011), which states that when film thickness is thin local tube curvature can be neglected.

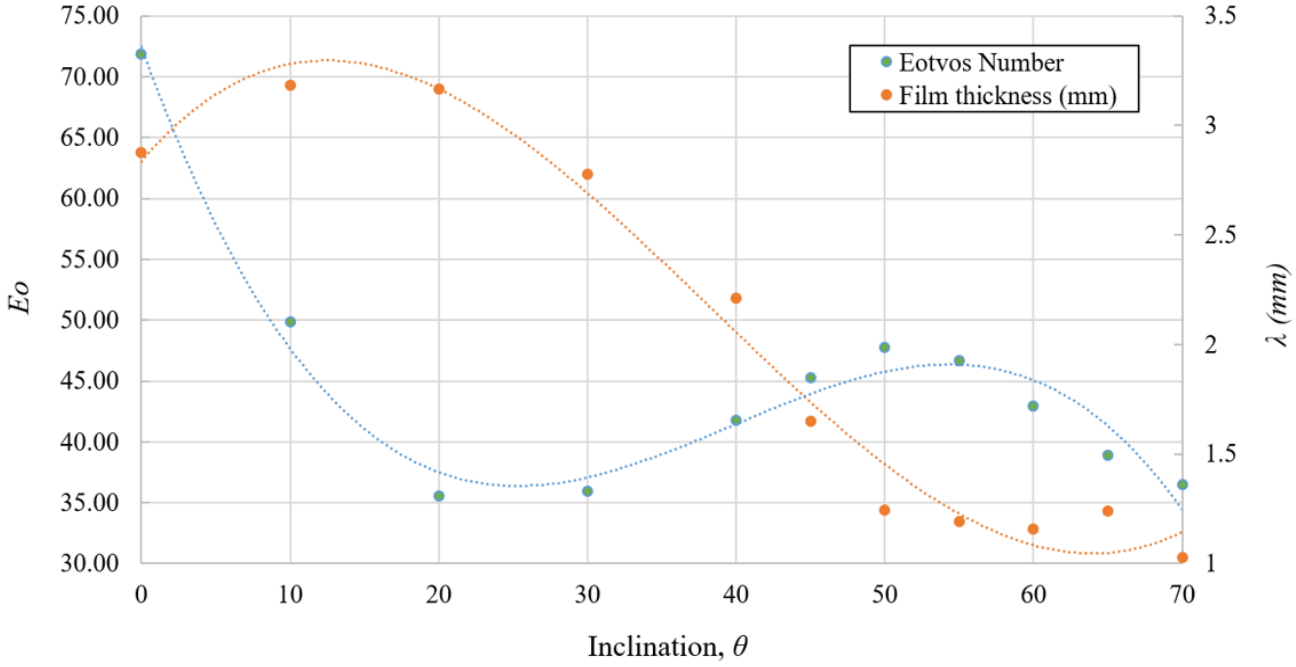

Figure 7: Graph shows Eotvos number and falling film thickness in water as a function of tube inclination for D = 0.027 m.

Film thickness decreases as the role of interfacial tension becomes more important, i.e., as *Eo* decreases, film thickness also decreases (Figure 8) and these occur alongside a decrease in N_f. High *Eo* values indicate that the system is relatively unaffected by interfacial tension, whereas a low value indicates that interfacial tension dominates (typically for $Eo < 1$). Therefore, the decreasing value of *Eo* with increasing inclination angle indicates an increasing dependence on inclination angle as buoyancy plays a larger role and pushes the bubble up against the upper

wall of the tube as inclination angle approaches 70°. Thinner falling films occur for liquids of low viscosities and film thickness increases with increasing viscosity, whereas large N_f and Re values give a thin falling film compared to pipe radius in vertical tubes. This observation is also consistent with inclined tubes, with the addition of film thickness also being a function of inclination. According to Bugg et al., (2002) film thickness is independent of Re and hence of ascent velocity for $10^{-5} \leq Re \leq 1$, meaning that for $Re > 2$ film thickness decreases as Reynolds number increases, which agrees with observations made in this study. Seyfried and Freundt (2000) states that film thickness is strongly dependent on Eo number for $Eo < 40$, and this dependence is more pronounced for smaller N_f values, i.e., more viscous liquids. As a result of this interfacial tension is negligible for $Eo > 40$ (Viana et al., 2003), which applies for most of this dataset as such only data for water (Figure 7) and olive oil (Figure 8) were plotted to show variation. Taylor bubbles cannot form when $Eo < 4$ because capillary forces restrict bubble movement (Bugg et al., 1998). While this may be relevant to studies on a laboratory scale, this cannot occur at a volcanic scale where conduit diameters are several meters wide.

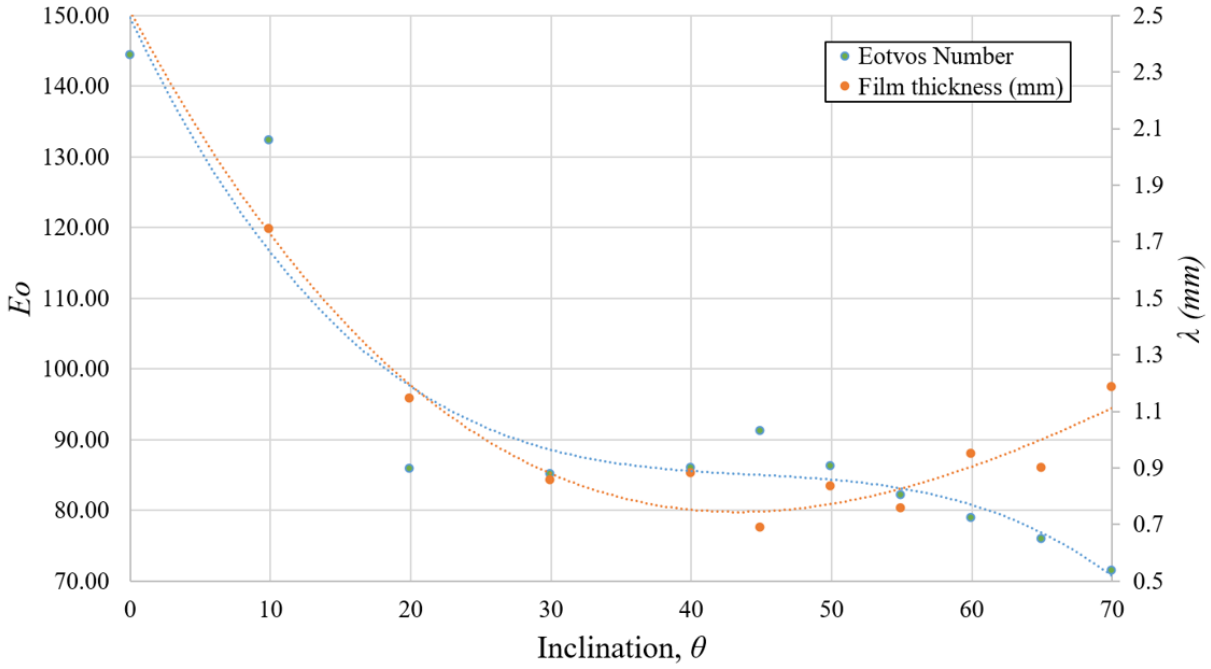

Figure 8: Graph shows Eotvos number and falling film thickness in olive oil as a function of tube inclination for D = 0.027 m.

3.5. Taylor Bubble Shape

A qualitative change in bubble geometry has been observed to occur in response to increasing inclination. Within tubes of vertical geometry bubble morphology is axisymmetric and the Taylor bubble ascends the pipe centre (Zukoski, 1966) and consistently with previous works

(Table 1), the shape of the nose and body remain qualitatively the same for both diameters in vertical tubes, i.e., when θ = 0, independent of bubble length. In Taylor bubbles the ratio of bubble to tube diameter is > 0.6, so tube diameter is the controlling length governing nose shape (de Azevedo et al., 2015), and as liquid viscosity increases, the shape of the bubble nose becomes blunter and velocity decreases. These observations also apply to inclined tubes in addition to a gradual change in bubble shape that is observed with increasing inclination. For all inclinations, including vertical, the bubble nose has a rounded shape, however, nose shape becomes more oblate, and the lower side of the bubble becomes flatter as the bubble lengthens and thins in response to an increased inclination angle. These observations are displayed in Figure 9 and agree with data from previous studies (Zukoski, 1966; James et al., 2004 Pokusaev et al., 2011). The influence of the contact angle of the slug on the tube wall affects bubble morphology; for θ = 0 (vertical) a standard stable bubble structure is observed across all N_f values, although turbulence can be observed in the wake for the range $7100 \leq N_f \leq 15560$ (water). This changes when θ > 0, where an asymmetric slug configuration above the tube's central axis is observed to occur as a function of inclination angle.

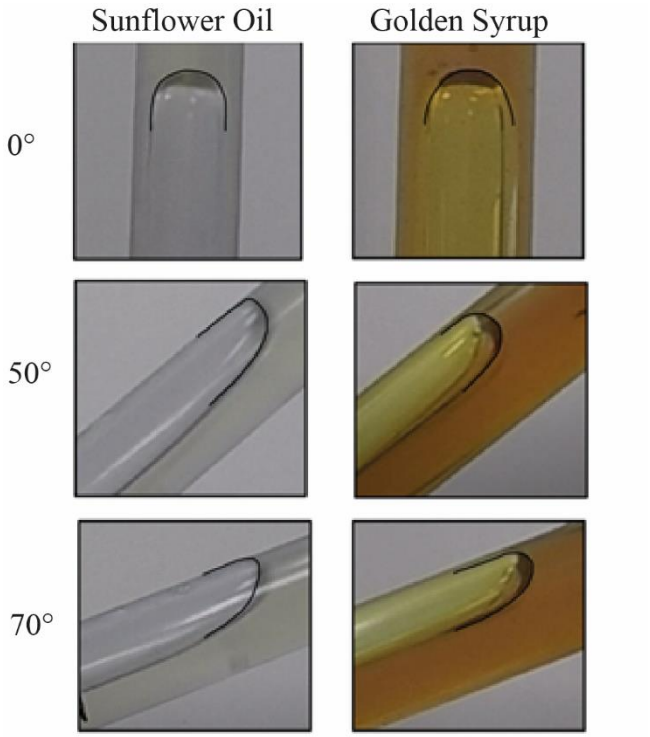

Figure 9: Photographs of Taylor bubble nose shape rising in sunflower oil (clear) and golden syrup (brown) where D = 0.027 m at inclination angles of 0° (vertical), 50° and 70°. Key morphologies have been outlined in black for clarity.

Tail morphology also changes for $\theta > 0$, especially for lower N_f values (Figure 10) where flow is less turbulent. Tail shape is thought to remain stable for $N_f \leq 600$ (Campos and de Carvalho, 1988; Viana et al., 2003; Llewellin et al., 2012), and results of this study show tail stability to be maintained up to $N_f = 101$, which possibly aligns with previous findings as the next highest data point for this dataset is $N_f = 7100$, meaning the value for stability lies within the range $101 \leq N_f \leq 7100$. Tail morphology is flat where viscous effects are unimportant and takes on the shape of an oblate spheroid where viscous effects become important in vertical tubes (Bugg et al., 1998), this also occurs with inclined tubes to an extent, however, tail shape becomes more wedge shaped or pointed at greater inclinations (Figure 10) for low and high viscosity liquids respectively.

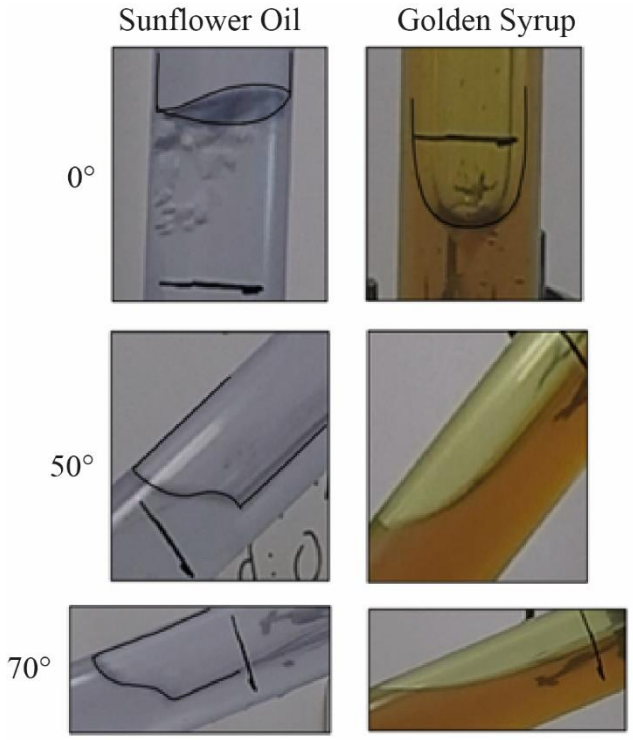

Figure 10: Photographs of Taylor bubble tail shape rising in sunflower oil (clear) and golden syrup (brown) where D = 0.027 m at inclination angles of 0° (vertical), 50° and 70°. Key morphologies have been outlined in black for clarity.

3.6. Taylor Bubble Ascent Velocity

Overall, Taylor bubble ascent velocity in vertical and inclined tubes is a function of the combination of liquid properties and tube geometry, meaning the propagation rate of volcanic Taylor bubbles is a result of magmatic properties and internal conduit geometry. For the full range of N_f velocity rates increase when inclination increases up to a maximum within the range $40 \leq \theta \leq 50$ for $D = 0.016$m and $50 \leq \theta \leq 60$ for $D = 0.027$ m before decreasing again (Figure 11).

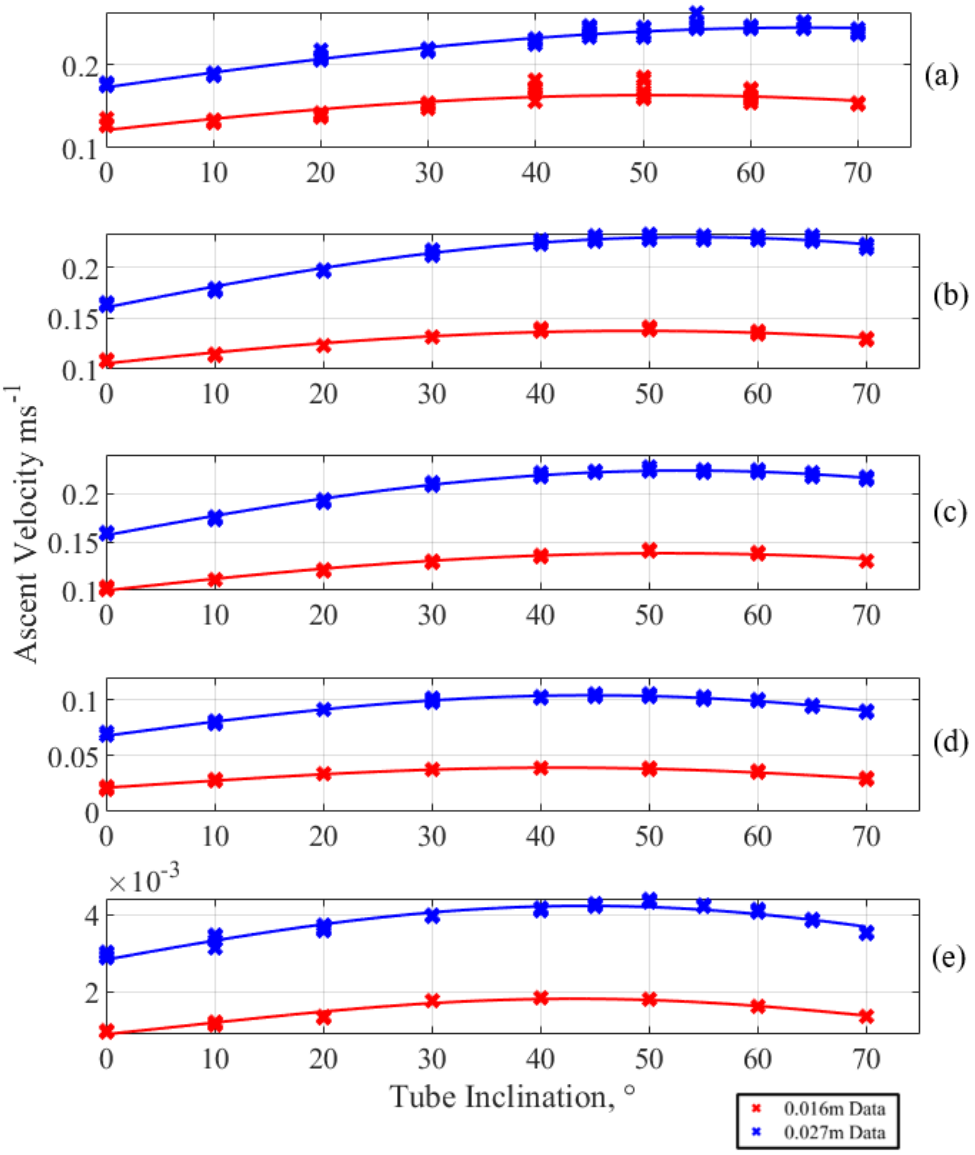

Figure 11: Taylor bubble ascent velocity as a function of tube inclination for both tube diameters in various Newtonian liquids: water (a), sunflower oil (b), olive oil (c), glycerol (d), and golden syrup (e).

For this study, only five different fluids were used, in two different pipe diameters, meaning this study covers ten N_f values of the range $0.5 < N_f < 15560$, however, only N_f values for the range $0.5 < N_f < 101$ were plotted given their volcanic relevance. The angle at which the maxima occurs for Taylor bubble ascent velocity is lower for low N_f than for high N_f (Figure 12), consistent with findings by Zukoski (1966) and Nigam et al., (1995). The effect of inclination angle on bubble rise velocity is complex and non-linear as a result of the observable change in bubble morphology that occurs in response to changes in inclination.

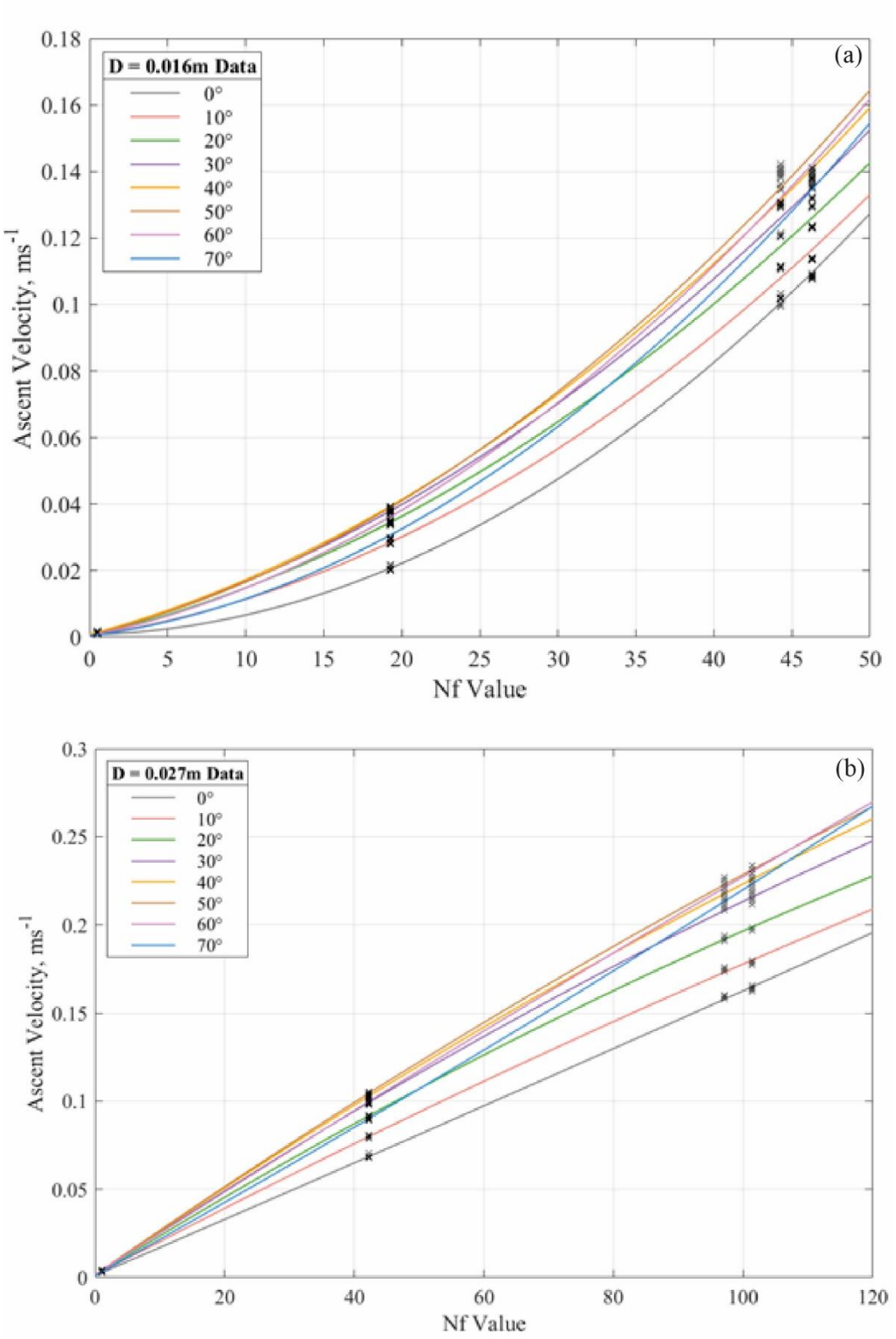

Figure 12: Taylor bubble ascent velocity as a function of N_f for (a) D = 0.016 m and (b) D = 0.027 m at every inclination angle.

As long as ascent velocity is independent of bubble length it is a function of the shape of the bubble head (Pokusaev et al., 2011), namely the curvature of the nose in the vicinity to its critical

point. This occurs when bubble length is > 1.5*D* (Shosho and Ryan, 2001; James et al., 2004). For less viscous liquids, inclination has negligible influence on bubble length generated from the same air volume, but a tendency of increasing bubble length is observed in liquids of high viscosity (or low N_f) when inclination increases. Changes in Taylor bubble structure, which is a

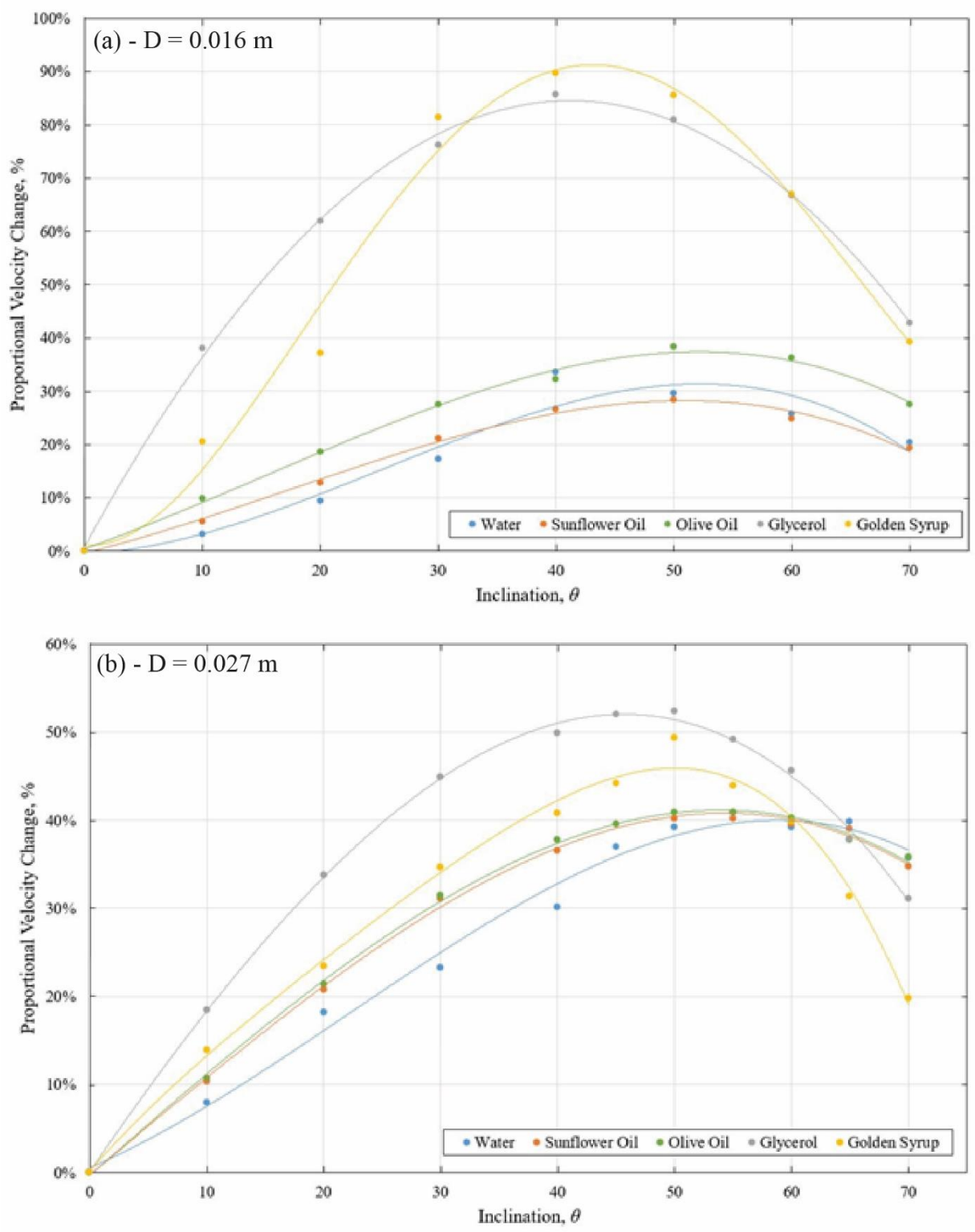

Figure 13: Proportional velocity change as a function of tube inclination for (a) D = 0.016 m, and (b) D = 0.027 m, for all liquids.

function of N_f and inclination, alters the overall drag coefficient and shape of the falling film surrounding the bubble and as a result influences the rate of ascent (Bugg et al., 1998). A system in laminar flow (low N_f, smaller diameter) increases the contribution of this viscous drag; this is displayed in Figure 13a where the maximum variation in proportional velocity change is observed to occur for D = 0.016 m at high viscosity ($0.5 \leq N_f \leq 19.3$), i.e., for golden syrup and glycerol. As flow regime becomes more turbulent (occurs with $D = 0.027$ m), the effect on proportional velocity change is smaller (Figure 13b).

3.7. Volcanic Context

These findings have a significant impact on the current knowledge of Taylor bubble dynamics in volcanic conduits, which are commonly assumed to contain vertical conduits in previous studies. Although this assumption is made on a purely theoretical basis, it is not a realistic approach to the study of bubble dynamics. Due to the nature of the trends displayed throughout this work. in comparison to data in Table 3, it can be assumed that the current ranges seen in literature for Taylor bubble flow on a volcanic scale would increase, specifically in reference to Taylor bubble ascent velocity rates and dimensionless parameters because the maximum value for each parameter always occurs at an inclination greater than 0° (vertical). Fr and Re are especially affected here, as they are direct functions of v_b (see equations [4] and [6]) which is a function of changing tube and therefore conduit scale inclination. These results also have specific implications for surface eruptive behaviour and controls on volcanic explosivity.

4. Conclusions

Here, we illustrated a simple and effective experimental approach that allows for the measurement of single Taylor bubbles ascending within both vertical and inclined conduits in two-phase flow. We derived and calculated dimensionless numbers and Taylor bubble flow characteristics in comparison to a natural volcanic scale. We highlight that Taylor bubble morphology is found to be a strong function of inclination, while the nose shape is a major controlling function for v_b for the full range of N_f studied here, especially when conduit inclination is within the range of $40 \leq \theta \leq 60$. We show a wider and higher range of v_b, Fr and Re (as function of inclination) than is presently seen in the current volcanic literature, which predominantly uses vertical conduit geometry to estimate Taylor bubble flow characteristics within volcanic conduits.

5. Acknowledgements

The authors would like to thank Alan Smalley and Joseph Hufton for their valuable assistance and guidance with experimental setup.

6. References

Amaya-Bower, L., Lee, T., 2010. Single bubble rising dynamics for moderate Reynolds number using Lattice Boltzmann Method. Comput. Fluids 39, 1191–1207. https://doi.org/10.1016/j.compfluid.2010.03.003

Barth, A., Edmonds, M., Woods, A., 2019. Valve-like dynamics of gas flow through a packed crystal mush and cyclic strombolian explosions. Sci. Rep. 9, 821. https://doi.org/10.1038/s41598-018-37013-8

Bendiksen, K.H., 1984. An experimental investigation of the motion of long bubbles in inclined tubes. Int. J. Multiph. Flow 10, 467–483. https://doi.org/10.1016/0301-9322(84)90057-0

Blackburn, E.A., Wilson, L., Sparks, R.S.J., 1976. Mechanisms and dynamics of strombolian activity. J. Geol. Soc. London. 132, 429–440. https://doi.org/10.1144/gsjgs.132.4.0429

Bugg, J.D., Saad, G.A., 2002. The velocity field around a Taylor bubble rising in a stagnant viscous fluid: Numerical and experimental results. Int. J. Multiph. Flow 28, 791–803. https://doi.org/10.1016/S0301-9322(02)00002-2

Campos, J.B.L.M., Carvalho, J.R.F.G. De, 1988. An experimental study of the wake of gas slugs rising in liquids. J. Fluid Mech. 196, 27. https://doi.org/10.1017/S0022112088002599

Capponi, A., James, M.R., Lane, S.J., 2016. Gas slug ascent in a stratified magma: Implications of flow organisation and instability for Strombolian eruption dynamics, Earth and Planetary Science Letters. https://doi.org/10.1016/j.epsl.2015.12.028

Chouet, B., Dawson, P., Ohminato, T., Martini, M., Saccorotti, G., Giudicepietro, F., De Luca, G., Milana, G., Scarpa, R., 2003. Source mechanisms of explosions at Stromboli Volcano, Italy, determined from moment-tensor inversions of very-long-period data. J. Geophys. Res. Solid Earth 108, 2019. https://doi.org/10.1029/2002JB001919

Chouet, B., Saccorotti, G., Martini, M., Dawson, P., De Luca, G., Milana, G., Scarpa, R., 1997. Source and path effects in the wave fields of tremor and explosions at Stromboli Volcano, Italy. J. Geophys. Res. 102, 15129–15150. https://doi.org/10.1029/97jb00953

de Azevedo, M.B., Santos, D. dos, Faccini, J.L.H., Su, J., 2016. Experimental study of the falling film of liquid around a Taylor bubble. Int. J. Multiph. Flow.

https://doi.org/10.1016/j.ijmultiphaseflow.2016.09.021

Del Bello, E., Lane, S.J., James, M.R., Llewellin, E.W., Taddeucci, J., Scarlato, P., Capponi, A., 2015. Viscous plugging can enhance and modulate explosivity of strombolian eruptions. Earth Planet. Sci. Lett. 423, 210–218. https://doi.org/10.1016/J.EPSL.2015.04.034

E. Shosho, C., E. Ryan, M., 2001. An experimental study of the motion of long bubbles in inclined tubes. Chem. Eng. Sci. 56, 2191–2204. https://doi.org/10.1016/S0009-2509(00)00504-2

Ilanko, T., Oppenheimer, C., Burgisser, A., Kyle, P., 2015. Transient degassing events at the lava lake of Erebus volcano, Antarctica: Chemistry and mechanisms. GeoResJ 7, 43–58. https://doi.org/10.1016/j.grj.2015.05.001

James, M.R., Lane, S.J., Chouet, B., Gilbert, J.S., 2004. Pressure changes associated with the ascent and bursting of gas slugs in liquid-filled vertical and inclined conduits. J. Volcanol. Geotherm. Res. 129, 61–82. https://doi.org/10.1016/S0377-0273(03)00232-4

James, M.R., Lane, S.J., Wilson, L., Corder, S.B., 2009. Degassing at low magma-viscosity volcanoes: Quantifying the transition between passive bubble-burst and Strombolian eruption. J. Volcanol. Geotherm. Res. 180, 81–88. https://doi.org/10.1016/j.jvolgeores.2008.09.002

Jaupart, C., Vergniolle, S., 1988. Laboratory models of Hawaiian and Strombolian eruptions. Nature 331, 58–60. https://doi.org/10.1038/331058a0

Kawaguchi, R., Nishimura, T., 2015. Numerical investigation of temporal changes in volcanic deformation caused by a gas slug ascent in the conduit. J. Volcanol. Geotherm. Res. 302, 1–10. https://doi.org/10.1016/j.jvolgeores.2015.06.002

Llewellin, E.W., Bello, E. Del, Taddeucci, J., Scarlato, P., Lane, S.J., 2012. The thickness of the falling film of liquid around a Taylor bubble The thickness of the falling film of liquid around. https://doi.org/10.1098/rspa.2011.0476

Marcos Bertrand de Azevedo, Douglas dos Santos, Nathalia Nunes Araujo, Pedro Andrade Maia Vinhas, José Luiz Horacio Faccini, Jian Su, 2015. Measurement of Interfacial Parameters of Single Taylor Bubbles Rising in Closed Vertical and Slightly Inclined Tubes Using Ultrasonic and Visualization Techniques., in: Proceedings of the 23rd ABCM International Congress of Mechanical Engineering. ABCM Brazilian Society of Mechanical Sciences and Engineering. https://doi.org/10.20906/cps/cob-2015-0479

Nigam, K.D.P., Pandit, A.B., Niranjan, K., 1995. Effect of angle of inclination on liquid-phase controlled mass transfer from a gas slug. Chem. Eng. Sci. 50, 289–298. https://doi.org/10.1016/0009-2509(94)00234-I

Nogueira, S., Riethmuller, M.L., Campos, J.B.L.M., Pinto, A.M.F.R., 2006. Flow patterns in the wake of a Taylor bubble rising through vertical columns of stagnant and flowing Newtonian liquids :

An experimental study 61, 7199–7212. https://doi.org/10.1016/j.ces.2006.08.002

Oppenheimer, J., Capponi, A., Cashman, K. V., Lane, S.J., Rust, A.C., James, M.R., 2020. Analogue experiments on the rise of large bubbles through a solids-rich suspension: A “weak plug” model for Strombolian eruptions. Earth Planet. Sci. Lett. 531, 115931. https://doi.org/10.1016/j.epsl.2019.115931

Parfitt, E.A., 2004. A discussion of the mechanisms of explosive basaltic eruptions. J. Volcanol. Geotherm. Res. 134, 77–107. https://doi.org/10.1016/j.jvolgeores.2004.01.002

Parfitt, E.A., Wilson, L., 1995. Explosive volcanic eruptions—IX. The transition between Hawaiian-style lava fountaining and Strombolian explosive activity. Geophys. J. Int. 121, 226–232. https://doi.org/10.1111/j.1365-246X.1995.tb03523.x

Pering, T.D., McGonigle, A.J.S., 2018. Combining Spherical-Cap and Taylor Bubble Fluid Dynamics with Plume Measurements to Characterize Basaltic Degassing. Geosciences 8, 42. https://doi.org/10.3390/geosciences8020042

Pering, T.D., McGonigle, A.J.S., James, M.R., Tamburello, G., Aiuppa, A., Delle Donne, D., Ripepe, M., 2016. Conduit dynamics and post explosion degassing on Stromboli: A combined UV camera and numerical modeling treatment. Geophys. Res. Lett. 43, 5009–5016. https://doi.org/10.1002/2016GL069001

Pering, T.D., McGonigle, A.J.S., Tamburello, G., Aiuppa, A., Bitetto, M., Rubino, C., Wilkes, T.C., 2017. A Novel and Inexpensive Method for Measuring Volcanic Plume Water Fluxes at High Temporal Resolution. Remote Sens. 9, 146. https://doi.org/10.3390/rs9020146

Pinto, A.M.F.R., Coelho Pinheiro, M.N., Campos, J.B.L.M., 1998. Coalescence of two gas slugs rising in a co-current flowing liquid in vertical tubes. Chem. Eng. Sci. 53, 2973–2983. https://doi.org/10.1016/S0009-2509(98)00121-3

Pokusaev, B.G., Kazenin, D.A., Karlov, S.P., Ermolaev, V.S., 2011. Motion of a gas slug in inclined tubes. Theor. Found. Chem. Eng. 45, 640–645. https://doi.org/10.1134/S0040579511050319

Seyfried, R., Freundt, A., 2000. Experiments on conduit flow and eruption behavior of basaltic volcanic eruptions. J. Geophys. Res. 105, 23727. https://doi.org/10.1029/2000JB900096

Sparks, R.S.J., 2003. Dynamics of magma degassing. Geol. Soc. London, Spec. Publ. 213, 5–22. https://doi.org/10.1144/GSL.SP.2003.213.01.02

Sparks, R.S.J., 1978. The dynamics of bubble formation and growth in magmas: A review and analysis. J. Volcanol. Geotherm. Res. 3, 1–37. https://doi.org/10.1016/0377-0273(78)90002-1

Spina, A. La, Burton, M.R., Harig, R., Mure, F., Rusch, P., Jordan, M., Caltabiano, T., 2013. New insights into volcanic processes at Stromboli from Cerberus , a remote-controlled open-path FTIR scanner system. J. Volcanol. Geotherm. Res. 249, 66–76.

https://doi.org/10.1016/j.jvolgeores.2012.09.004

Taddeucci, J., Edmonds, M., Houghton, B., James, M.R., Vergniolle, S., 2015. Hawaiian and Strombolian Eruptions, in: The Encyclopedia of Volcanoes. Elsevier, pp. 485–503. https://doi.org/10.1016/b978-0-12-385938-9.00027-4

Vergniolle, S., Jaupart, C., 1990. Dynamics of degassing at Kilauea Volcano, Hawaii. J. Geophys. Res. 95, 2793. https://doi.org/10.1029/JB095iB03p02793

Vergniolle, S., Jaupart, C., 1986. Separated two-phase flow and basaltic eruptions. J. Geophys. Res. Solid Earth 91, 12842–12860. https://doi.org/10.1029/JB091iB12p12842

Viana, F., Pardo, R., Yánez, R., Trallero, J.L., Joseph, D.D., 2003. Universal correlation for the rise velocity of long gas bubbles in round pipes. J. Fluid Mech. 494, 379–398. https://doi.org/10.1017/S0022112003006165

Wilson, L., Head, J.W., 1981. Ascent and eruption of basaltic magma on the Earth and Moon. J. Geophys. Res. Solid Earth 86, 2971–3001. https://doi.org/10.1029/JB086iB04p02971

Woitischek, J., Edmonds, M., Woods, A.W., 2020. the control of magma crystallinity on the fluctuations in gas composition at open vent basaltic volcanoes 10, 14862. https://doi.org/10.1038/s41598-020-71667-7

Zukoski, E.E., 1966. Influence of viscosity, surface tension, and inclination angle on motion of long bubbles in closed tubes. J. Fluid Mech. 25, 821–837. https://doi.org/10.1017/S0022112066000442